Adhesion induced buckling of spherical shells

2004 J. Phys.: Condens. Matter 16 L421

(http://iopscience.iop.org/0953-8984/16/39/L01)

INSTITUTE OF PHYSICS PUBLISHING JOURNAL OF PHYSICS: CONDENSED MATTER

J. Phys.: Condens. Matter **16** (2004) L421–L428 PII: S0953-8984(04)83466-0

LETTER TO THE EDITOR

Adhesion induced buckling of spherical shells

K Tamura, S Komura and T Kato

Department of Chemistry, Faculty of Science, Tokyo Metropolitan University, Tokyo 192-0397, Japan

Received 12 July 2004, in final form 31 August 2004
Published 17 September 2004
Online at stacks.iop.org/JPhysCM/16/L421
doi:10.1088/0953-8984/16/39/L01

Abstract

Deformation of a spherical shell adhering onto a rigid substrate due to van der Waals attractive interaction is investigated by means of numerical minimization of the sum of the elastic and adhesion energies. The conformation of the deformed shell is governed by two dimensionless parameters C_s/ϵ and C_b/ϵ, where C_s and C_b are respectively the stretching and the bending constants, and ϵ is the depth of the van der Waals potential. As a function of C_b/ϵ, we find both continuous and discontinuous buckling transitions for small and large C_s/ϵ, respectively, which is analogous to van der Waals fluids or gels. Some scaling arguments are employed to explain the adhesion induced buckling transition.

Deformation of thin elastic sheets such as graphitic oxide [1], polymerized Langmuir monolayers [2], or cytoskeletons of biological cell membranes [3] has attracted considerable interest in recent years. From the theoretical viewpoint, scaling properties of stretching ridges in a crumpled elastic sheet were investigated by analysing the nonlinear Föppl–von Kármán (FvK) equations [4]. The FvK equations for plates have been the subject of renewed interest in the context of developable cone (d-cone) singularities [5], pattern formations induced by buckling [6], or formations of plastic tears [7]. However, most of these works are concerned with *flat* elastic sheets, while less attention has been paid to the properties of initially *curved* elastic sheets, i.e., *shells*.

Quite generally, curved shells exhibit a peculiar elastic feature because the stretching is a first-order effect and they cannot be bent without being stretched [8]. This interplay between bending and stretching, leading to a reduced flexibility of the shell, was studied for thermal fluctuations of polymerized vesicles [9] or the asymptotic shape of fullerenes [10]. In the previous paper, the deformation and mechanical stability of fullerene-like hollow nanoparticles were investigated within the shell theory [11]. It was shown that van der Waals (vdW) interaction between a rigid substrate and nanoparticles can cause considerable deformation of the latter. A similar problem was studied for elastic tubes by means of a numerical approach and a scaling theory [12]. As for the experiments on shells, a buckling instability of self-assembled actin-coated vesicles was observed under the application of a localized force using

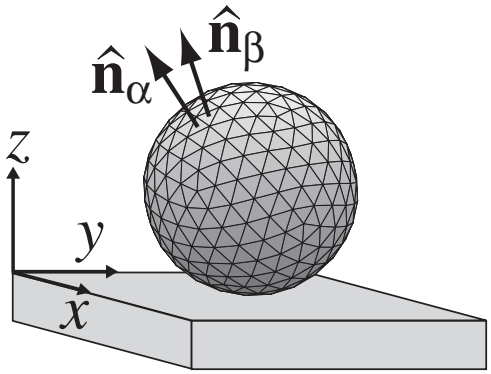

Figure 1. Bead and spring model of an elastic spherical shell adhering onto a substrate. $\hat{\mathbf{n}}_{\alpha(\beta)}$ is the unit normal vector of the triangle $\alpha(\beta)$.

optical tweezers [13]. Recently, the elastic properties of polyelectrolyte microcapsules were studied by using AFM [14]. At the macroscopic level, the contact and compression problem of ping-pong and tennis balls was investigated in [15].

In this letter, we report a new type of instability that is found for spherical shells interacting with a rigid substrate: namely the buckling transition induced by adhesion. We investigate both numerically and theoretically the deformation of a spherical shell adhering onto a rigid substrate due to vdW attractive interaction. Our work can be regarded in part as a contact problem of spherical shells. Although the solution by Hertz for the contact problem of elastic bodies is well known [8], there have been only a few works which deal with the corresponding problem of shells. On the other hand, the present study is important for such as tribological applications of fullerene-like balls since there is little control over the shape of adsorbed nanoparticles [11]. We find both continuous and discontinuous buckling transitions for weak and strong adhesion cases, respectively. Moreover, creation of a polygonal structure is observed when the adhesion is strong enough. These results are compared with the experimentally observed buckling instability of a ping-pong ball which is pressed against a rigid plate [15]. Based on the continuum elastic theory, we also discuss the scaling theory of the observed buckling transition.

Consider an elastic spherical shell interacting with a rigid substrate as shown in figure 1. The normal direction to the substrate is taken as the z-axis, whereas the substrate spans the xy-plane. The initial configuration of the shell consists of a spherically closed triangular mesh as a simplest approximation for two-dimensional elastic materials. To generate such a structure, we start from an icosahedron as the original network, and add new points on each triangle followed by a subsequent rescaling of all bonds to the desired length [16]. This procedure ensures that most of the grid points have six neighbours and each bond has approximately the same length. We then associate all the grid points and bonds with beads and springs, respectively. In the present work, we used a spherical shell consisting of $N = 812$ beads among which there are 12 beads having five neighbours[1].

To describe the deformations of an elastic shell, both the stretching and the bending energies should be taken into account [8]. Following the model of membranes with crystalline order [17], or crushed elastic manifolds [18], the discretized stretching energy is given by the

[1] The numbers of triangles and springs are 1620 and 2430, respectively.

sum over Hooke's law of each spring:

$$E_{\mathrm{s}} = \sum_{n} \frac{1}{2} C_{\mathrm{s}} \left(\frac{L_n - L_0}{L_0} \right)^2 . \tag{1}$$

Here C_{s} is the stretching constant, L_n is the length of spring n, and L_0 is the natural length of the spring. On the other hand, the discretized bending energy is calculated according to [17, 18]

$$E_{\mathrm{b}} = \sum_{\langle \alpha\beta \rangle} \tfrac{1}{2} C_{\mathrm{b}} |\hat{\mathbf{n}}_\alpha - \hat{\mathbf{n}}_\beta|^2, \tag{2}$$

where C_{b} is the bending constant, $\hat{\mathbf{n}}_{\alpha(\beta)}$ is the unit normal vector of triangle $\alpha(\beta)$, and the sum is taken over each pair of triangles which share a common edge. We comment that both C_{s} and C_{b} have the dimension of energy.

The adhesion energy of the shell is included through the vdW interaction between each of the bead and the substrate [12]:

$$W = \sum_{i} \frac{2^{8/3}}{3} \epsilon \left[\left(\frac{\sigma}{z_i} \right)^{12} - \left(\frac{\sigma}{z_i} \right)^{3} \right], \tag{3}$$

where z_i is the height of bead i from the substrate. When the adhesion energy of bead i is plotted against z_i, the depth of the energy minimum is given by ϵ, and the distance corresponding to this minimum is $2^{2/9}\sigma$. The first repulsive term in equation (3) is responsible for the excluded volume interaction which prevents the beads from penetrating into the substrate. The second term represents the long-ranged attractive interaction between the beads and the substrate [19]. Notice that the inverse cubic dependence results from the pairwise additivity of the vdW interaction between two atoms.

The total energy $E_{\mathrm{tot}} = E_{\mathrm{s}} + E_{\mathrm{b}} + W$ is numerically minimized using the conjugate gradient method [20]. Hereafter all the energies and the lengths are respectively scaled by ϵ and σ which characterize the vdW interaction in equation (3). There are three independent dimensionless parameters in the model, i.e., C_{s}/ϵ, C_{b}/ϵ, and L_0/σ. In the present study, we have mainly varied C_{s}/ϵ and C_{b}/ϵ. The natural length of each bond L_0/σ is chosen such that the initial configuration of the shell does not store any stretching energy, and its value is roughly $L_0/\sigma \approx 0.1$. For $N = 812$, the scaled radius of the undeformed shell is $R/\sigma \approx 0.75$. We note that the bending energy is inherent even in the undeformed shell since the spontaneous curvature is not included in the present calculation. This assumption is justified such as for fullerene balls.

Figure 2 shows various typical final configurations of the adhering shell as the combination of C_{s}/ϵ and C_{b}/ϵ is varied. There are four qualitatively distinct patterns of deformation as classified from (a) to (d) in figure 2. For case (a) when both C_{s}/ϵ and C_{b}/ϵ are large enough, the shell hardly deforms in spite of the adhesion, and keeps its spherical shape. As both values are reduced, we observe case (b) where a flat contact disc develops at the bottom of the shell. Further decrease of C_{b}/ϵ results in the buckling of the shell as illustrated in case (c). In such a configuration, both the stretching and the bending energies are localized at a narrow 'bending strip' of contact. For case (d) with smaller C_{b}/ϵ, it becomes energetically favourable to create a polygonal structure composed of a number of ridges joined by the d-cones. The number of ridges (four in the case of (d)) depends on the strength of the vdW attraction, which will be reported separately. In contrast to spherical shells, the buckling phenomenon has never been observed for elastic tubes [12].

In order to quantify the observed deformation, we employ the moment of inertia tensor calculated by

$$I_{pq} = \frac{1}{2N^2} \sum_{i} \sum_{j} (r_{i,p} - r_{j,p})(r_{i,q} - r_{j,q}), \tag{4}$$

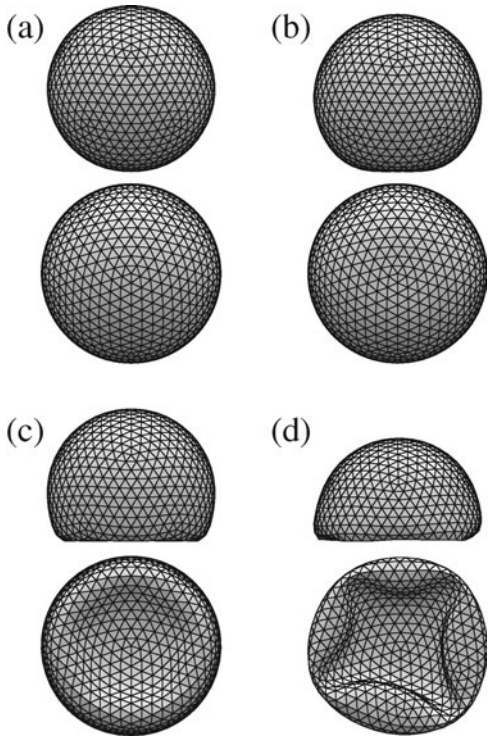

Figure 2. Side and bottom views of the adhering spherical shells which have the minimized total energy $E_{\rm tot}$ when the sets of the scaled elastic constants $(C_{\rm s}/\epsilon, C_{\rm b}/\epsilon)$ are (a) (1000, 1000), (b) (150, 9), (c) (150, 2), and (d) (100, 1.1).

where $\mathbf{r}_i$ is the position of bead i, and $p, q = x, y, z$. The three eigenvalues of I_{pq} are ordered according to magnitude $\lambda_1 \leqslant \lambda_2 \leqslant \lambda_3$. As a quantitative measure of the anisotropy of the deformed shell, we have calculated [21]

$$\Delta = \frac{\lambda_1^2 + \lambda_2^2 + \lambda_3^2 - (\lambda_1\lambda_2 + \lambda_2\lambda_3 + \lambda_3\lambda_1)}{(\lambda_1 + \lambda_2 + \lambda_3)^2}. \tag{5}$$

This quantity vanishes for an isotropic configuration, but it deviates from zero when the shell undergoes anisotropic deformations. In figure 3 we have plotted Δ as a function of $C_{\rm b}/\epsilon$ for various different values of $C_{\rm s}/\epsilon$. The buckling of the shell is manifested in the sharp increase of Δ as $C_{\rm b}/\epsilon$ is decreased. There are even jumps of Δ for larger values of $C_{\rm s}/\epsilon$, which indicates the occurrence of a discontinuous buckling transition. It is worthwhile to mention that Δ attains its minimum at $C_{\rm b}/\epsilon$ larger than its threshold value of the buckling.

For $C_{\rm s}/\epsilon = 300$, we have plotted in figure 4 all the minimized energies, equations (1)–(3), and the total energy $E_{\rm tot}$ as a function of $C_{\rm b}/\epsilon$. In this case, the shell exhibits a discontinuous buckling transition at around $(C_{\rm b}/\epsilon)^* \approx 5$ as indicated by the dashed line. When the value of $C_{\rm b}/\epsilon$ crosses this critical value from above, both the stretching energy $E_{\rm s}$ and the bending energy $E_{\rm b}$ increase abruptly. These losses in the elastic energies are compensated by the gain in the vdW energy W which decreases discontinuously at the transition point. In other words, the shell buckles at the expense of the elastic energy when the adhesive force is strong enough. Interestingly, however, we do not see any apparent discontinuity in $E_{\rm tot}$ around the transition point. For different values of $C_{\rm s}/\epsilon$, the behaviours of each energy are qualitatively the same when the discontinuous buckling occurs.

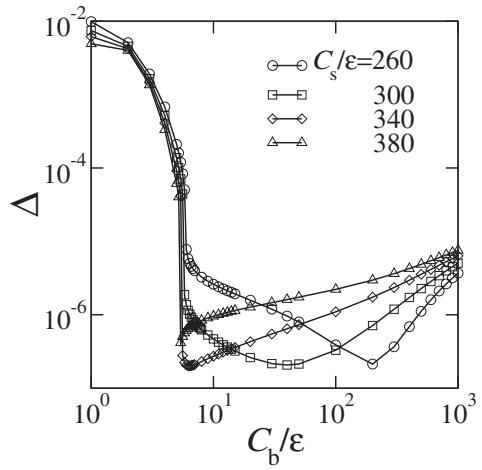

Figure 3. The anisotropy factor Δ defined in equation (5) as a function of the scaled bending constant C_b/ϵ for various values of C_s/ϵ ranging from 260 to 380.

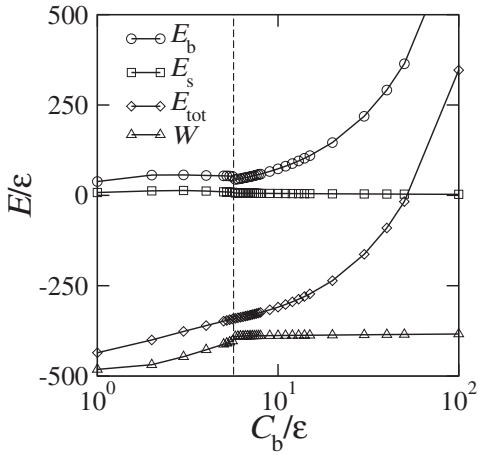

Figure 4. The minimized total energy E_{tot}/ϵ as a function of C_b/ϵ when $C_s/\epsilon = 300$. The three energies E_s, E_b, and W contributing to E_{tot} are also shown. The discontinuous buckling transition occurs at $(C_b/\epsilon)^* \approx 5$ indicated by the dashed line.

To investigate the property of the buckling transition in more detail, we have measured the indentation length H which is defined in the inset of figure 5. The same figure shows the scaled indentation length H/R as a function of C_b/ϵ for various C_s/ϵ ranging from 100 to 900. In accordance with the aforementioned discussion, H changes discontinuously at the transition point for larger C_s/ϵ, revealing the first-order nature of the buckling transition. This discontinuous buckling transition takes place between the configurations, figures 2(b) and (c), i.e., the contact region changes from a disc to a ring at the transition point. However, the discontinuous jump in H becomes smaller as C_s/ϵ is decreased, and finally vanishes at around $C_b/\epsilon \approx 6.1$ (the filled circle). The corresponding critical indentation length is $H/R \approx 0.18$, and that of the stretching constant is $C_s/\epsilon \approx 210$. Below this value of C_s/ϵ, the buckling occurs continuously between the two configurations (figures 2(b) and (c)). We immediately

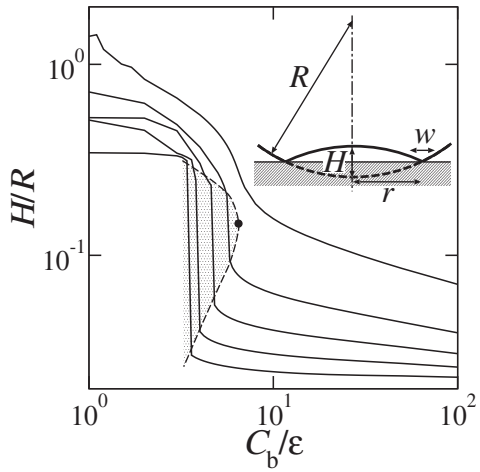

Figure 5. The relative indentation length H/R as a function of C_b/ϵ for various C_s/ϵ ranging from 100 (top) to 900 (bottom) for every 200. The discontinuous buckling occurs in the shaded region. The filled circle located roughly at $(C_b/\epsilon, H/R, C_s/\epsilon) = (6.1, 0.18, 210)$ indicates the point at which the discontinuity vanishes. The inset defines the geometry of the deformed spherical shell (see the text).

note that figure 5 is very reminiscent of the isotherms of vdW fluids. Analogous to the liquid–gas coexistence region, the region of discontinuous transition has been shaded in figure 5. In the present model, the parameter C_s/ϵ plays a role similar to the temperature of vdW fluids. Another similar phenomenon is the volume transition of gels which is induced either by changing the temperature or the ionic strength.

When the size of the shell N is changed, the indentation length H behaves similarly to figure 5 although the location of the critical point shifts systematically. Roughly speaking, the critical values of the elastic constants become larger for bigger shells as long as the potential range satisfies $R/\sigma \leqslant 1$. When this ratio is much larger than unity, the buckling does not occur. Details of the size effect will also be published elsewhere.

We now pay attention to cases (b) and (c) in figure 2, and interpret the corresponding deformations within the scaling argument [8]. Notice again that the buckling transition corresponds to the transition between these two configurations. In the following continuum treatment, we use C_s/L_0^2 to be the two-dimensional Young's modulus, C_b the bending rigidity as our discretized model. Then the effective thickness of the shell is expressed as $h = (8C_bL_0^2/C_s)^{1/2}$ [17]. As shown in figure 2(b), the shell deforms only slightly at the bottom when the adhesive force is weak. Let d be the dimension of the deformed region which is caused by the contact with the substrate. Following the case of a shell subjected to a small localized force [8], we balance the associated stretching and bending energies to obtain $d \sim (C_bL_0^2/C_s)^{1/4}R^{1/2}$. Hence the area of the contact region $S^{(b)}$ scales as

$$S^{(b)} \sim d^2 \sim (C_bL_0^2/C_s)^{1/2}R. \tag{6}$$

For strong adhesion, on the other hand, the buckling takes place as in figure 2(c), and most of the elastic energies are concentrated over a narrow 'bending strip' of width w and radius r (see the inset of figure 5). Applying the case of a large deformation also described in [8], we obtain $w \sim (C_bL_0^2/C_s)^{1/4}R^{1/2}$ and $r \sim H^{1/2}R^{1/2}$. Note that the scalings for d and w are the same. The area of the bending strip that contacts with the substrate is then given as

$$S^{(c)} \sim wr \sim (C_bL_0^2/C_s)^{1/4}H^{1/2}R. \tag{7}$$

Comparing equations (6) and (7), we see that the contact area of the bending strip becomes larger when $H > (C_b L_0^2/C_s)^{1/2} \sim h$, namely, when the indentation length exceeds the effective shell thickness. The increase in the contact area between the shell and the substrate results in the gain in the vdW adhesion energy, and hence W decreases when the buckling takes place as shown figure 4. The 'critical point' in figure 5 corresponds to the elastic constants $C_b/\epsilon \approx 6.1$ and $C_s/\epsilon \approx 210$ from which the effective thickness is calculated as $h/R \approx 0.064$. Since the numerically obtained critical indentation length is $H/R \approx 0.18$, we have $H \approx 2.8h$ at this point. This result indeed confirms the fact that the buckling transition takes place when the indentation length exceeds the shell thickness.

Experimentally, Pauchard and Rica studied the deformation of a ping-pong ball which is forced to be in contact with a rigid plate [15]. In their work, the boundary of the half-sphere was fixed in order to avoid non-axisymmetric deformations. For low applied forces, the shell flattens against the horizontal plate. For higher compression forces, the discontinuous buckling transition occurs when a deformation is close to twice the thickness of the shell ($H \approx 2.4h$). Although their experimental set-up is not identical to our model of adhesion, these behaviours are in excellent agreement with our simulation results. However, the occurrence of the continuous buckling transition of the shell with small stretching constant is our new finding.

For comparison with other adhesion experiments, we give below some numbers to the model parameters. For a layered material made of carbon, the two-dimensional Young's modulus and the bending rigidity are roughly 1.3×10^5 erg cm^{-2} and 1.6×10^{-12} erg, respectively [22]. Assuming that the adhesion energy ϵ is of the order of thermal energy $k_B T$, we can deduce the model parameters as $C_s/\epsilon \approx 480$ and $C_b/\epsilon \approx 40$. According to figure 5, the adhesion of a single-walled fullerene with radius $R/\sigma \approx 0.75$ should correspond to a point well above the critical point. In this regime, the fullerene may deform as in figure 2(b), which is consistent with the previous prediction [11]. Another example is the adhesion of a hollow polyelectrolyte microcapsule onto a flat substrate [14]. The three-dimensional Young's modulus of this shell material was measured to be in the range of 1.5–2 GPa, but its thickness h tends to be in the 10 nm range. Since this gives fairly large bending rigidity of the order of $C_b/\epsilon \approx 10^4$, we expect that a microcapsule would hardly deform due to vdW adhesion as in figure 2(a). However, other attractive interaction such as electrostatic interaction can lead to adhesion induced buckling of microcapsules [14].

We have investigated the deformation of an elastic shell adhering onto a rigid substrate by using the conjugate gradient method and the scaling argument. We find that both the discontinuous and the continuous bucking transitions occur for large and small stretching constants, respectively. Further studies such as the analysis of the ridges and d-cones in the strongly deformed region, or a spherical shell with a spontaneous curvature, are under progress.

We thank S A Safran for useful discussions. This work is supported by the Ministry of Education, Culture, Sports, Science and Technology, Japan (Grant-in-Aid for Scientific Research No. 15540395).

References

[1] Spector M S, Naranjo E, Chiruvolu S and Zasadzinski J A 1994 *Phys. Rev. Lett.* **73** 2867
[2] Saint-Jalmes A and Gallet F 1998 *Eur. Phys. J.* B **2** 489
[3] Schmidt C F, Svoboda K, Lei N, Petsche I B, Berman L E, Safinya C R and Grest G S 1993 *Science* **259** 952
[4] Lobkovsky A E, Gentges S, Li H, Morse D and Witten T A 1995 *Science* **270** 1482
Lobkovsky A E 1996 *Phys. Rev.* E **53** 3750

DiDonna B A 2002 *Phys. Rev.* E **66** 016601
[5] Ben Amar M and Pomeau Y 1997 *Proc. R. Soc.* A **453** 729
Cerda E, Chaieb S, Melo F and Mahadevan L 1999 *Nature* **401** 46
Boudaoud A, Patrício P, Couder Y and Ben Amar M 2000 *Nature* **407** 718
[6] Audoly B, Roman B and Pocheau A 2002 *Eur. Phys. J.* B **27** 7
Audoly B and Boudaoud A 2003 *Phys. Rev. Lett.* **91** 086105
[7] Marder M, Sharon E, Smith S and Roman B 2003 *Europhys. Lett.* **62** 498
[8] Landau L D and Lifshitz E M 1986 *Theory of Elasticity* (Oxford: Pergamon)
[9] Komura S and Lipowsky R 1992 *J. Physique* II **2** 1563
[10] Witten T A and Li H 1993 *Europhys. Lett.* **23** 51
[11] Schwarz U S, Komura S and Safran S A 2000 *Europhys. Lett.* **50** 762
[12] Komura S, Tamura K and Kato T 2004 *Eur. Phys. J.* E **13** 73
[13] Helfer E, Harlepp S, Bourdieu L, Robert J, MacKintosh F C and Chatenay D 2001 *Phys. Rev. Lett.* **87** 088103
[14] Dubreuil F, Elsner N and Fery A 2003 *Eur. Phys. J.* E **12** 215
Elsner N, Dubreuil F and Fery A 2004 *Phys. Rev.* E **69** 031802
[15] Pauchard L, Pomeau Y and Rica S 1997 *C. R. Acad. Sci.* **324** 411
Pauchard L and Rica S 1998 *Phil. Mag.* B **78** 225
[16] Komura S and Baumgärtner A 1991 *Phys. Rev.* A **44** 3511
[17] Seung H S and Nelson D R 1988 *Phys. Rev.* A **38** 1005
[18] Kramer E M and Witten T A 1997 *Phys. Rev. Lett.* **78** 1303
[19] Israelachivili J N 1991 *Intermolecular and Surface Forces* (London: Academic)
[20] Press W H, Flannery B P, Teukolsky S A and Vetterling W T 1989 *Numerical Recipes* (New York: Cambridge University)
[21] Gompper G and Kroll D M 1992 *Phys. Rev.* A **46** 7466
[22] Tersoff J 1992 *Phys. Rev.* B **46** 15546